Available online at www.sciencedirect.com
SCIENCE DIRECT®
Catalysis Today 96 (2004) 135–141
CATALYSIS TODAY
www.elsevier.com/locate/cattod

Tertiary butylation of phenol over mesoporous MeMCM-48 and MeMCM-41 (Me = Ga, Fe, Al or B) solid acid catalysts

P. Selvam*, S.E. Dapurkar

Solid State and Catalysis Laboratory, Department of Chemistry, Indian Institute of Technology-Bombay, Powai, Mumbai 400 076, India

Available online 17 July 2004

Abstract

Mesoporous Na-GaMCM-48 molecular sieves having a silicon-to-gallium (molar) ratio of 30–90 were synthesized hydrothermally, and the structure, coordination geometry of the gallium, acidic properties, and catalytic activity were systematically investigated using a number of analytical and spectroscopic techniques. XRD, TEM and N_2 sorption investigations indicate an MCM-48 structure with highly ordered mesoporosity. ^{71}Ga MAS-NMR studies reveal that gallium substitutes isomorphously in the mesoporous silicate framework of MCM-48. The NH_3-TPD profiles suggest the presence of high concentrations of moderate-to-strong Brønsted acid sites in H-GaMCM-48. The catalytic performance of this protonated catalyst was evaluated for the *t*-butylation of phenol. The results indicate that the H-GaMCM-48 catalysts are highly active for the chosen reaction, and show much higher substrate conversion than many other catalyst systems. However, compared to the analogous H-GaMCM-41, the H-GaMCM-48 shows a slight decrease in *p-t*-butyl phenol selectivity owing to the formation of 2,4-di-*t*-butyl phenol. On the other hand, the deactivation is very minimal on account of the three-dimensional pore system of the MCM-48 structure compared to the one-dimensional pore opening of the MCM-41 structure.

Keywords: Mesoporous materials; Molecular sieve catalyst; GaMCM-48; *tertiary*-Butyl phenol; Alkylation

1. Introduction

The discovery of thermally stable mesoporous silicate molecular sieves [1] having one-dimensional hexagonal MCM-41 and three-dimensional cubic MCM-48 structures has attracted significant research interest, and opened up new opportunities in many areas, in particular, heterogeneous catalysis [2–6]. However, much attention has been devoted on the catalytic properties of metal-containing MCM-41 structure, but only very little attention has been paid on the catalytic properties of metal-incorporating MCM-48 materials [7–10], probably because of the difficulties to synthesize good quality samples because of the narrower homogeneity region of the MCM-48 phase [11]. On the other hand, with the inherent benefit of a three-dimensional pore structure, as well as the associated advantage of the resistance against pore blockage, MCM-48 could serve as an excellent candidate for catalytic applications [7,12–18]. For example, the isopropylation of naphthalene and pyrene over H-AlMCM-48 exhibits much higher activity than H-AlMCM-41 [19]. However, it is noteworthy that only very few reports are available on the catalytic properties of mesoporous gallosilicates [9,10,20–24]. Therefore, in this investigation, an attempt has been made to synthesize and characterize high quality GaMCM-48, and to evaluate its catalytic ability for the *tertiary*-butylation (*t*-butylation) reaction of phenol as the products, viz., *para-tertiary*-butyl phenol (*p-t*-BP) and 2,4-di-*tertiary*-butyl phenol (2,4-di-*t*-BP), are industrially important [25]. In addition, like many other porous solids acid catalysts, e.g. H-Y [26], H-ZSM-12 [27], SAPO-11 [28], H-AlMCM-41 [29,30], H-FeMCM-41 [31], H-GaMCM-41 [32], and H-AlMCM-48 [16], the mesoporous H-GaMCM-48 also possess moderate acidic sites which is expected to favor the chosen reaction. For a comparative study, we have also included the results of both MeMCM-48 (Me = B, Al and Fe) and MeMCM-41 (Me = B, Al, Ga and Fe) catalysts.

2. Experimental

2.1. Starting materials

Gallium nitrate nonahydrate ($Ga(NO_3)_3{\cdot}9H_2O$; Aldrich; 98%), tetraethylorthosilicate (TEOS; Aldrich; 98%) and

* Corresponding author. Tel.: +91 22 576 7155; fax: +91 22 572 3480.
E-mail address: selvam@iitb.ac.in (P. Selvam).

0920-5861/$ – see front matter © 2004 Elsevier B.V. All rights reserved.
doi:10.1016/j.cattod.2004.06.114

cetyltrimethylammonium bromide (CTAB; Aldrich; 99%) were used as sources for gallium, silicon, and as template, respectively, and sodium hydroxide (NaOH; Loba; 98%) was used as alkali source. Phenol (Merck; 99.5%), *tertiary*-butyl alcohol (*t*-BA; Thomas Baker; 99%) were used for the vapour phase phenol alkylation reactions. Authentic samples of *ortho-tertiary*-butyl phenol (*o-t*-BP; Fluka; 99%), *meta-tertiary*-butyl phenol (*m-t*-BP; Aldrich; 99%), *para-tertiary*-butyl phenol (*p-t*-BP; Fluka; 99%), and 2,4-di-*tertiary*-butyl phenol (2,4-di-*t*-BP; Fluka; 99%) were used for comparative analyses of the reaction products.

2.2. Synthesis of Na-GaMCM-48

The sodium-form of GaMCM-48 was synthesized as per the following procedure with a typical molar gel composition of: SiO_2:0.25 $(Na_2O)_2$:0.30 $(CTA)_2O$:60 H_2O:0.0083 Ga_2O_3. A solution 'A' was obtained by mixing NaOH and tetraethyl orthosilicate (TEOS) in distilled water under constant stirring for 10 min. Solution 'B' was prepared by dissolving CTAB in distilled water, and was stirred for 20 min. Finally, a homogeneous transparent gel was obtained by mixing the solutions 'A' and 'B' under constant stirring for 25 min. To the resulting gel, the gallium source was added, and the mixture stirred for an additional hour for homogenization. The pH of final gel was 11.4. This was then subjected to hydrothermal treatment at 383 K for 72 h. The solid as-synthesized product was washed repeatedly, filtered and dried at 353 K for 12 h, and calcined at 823 K for 2 h in N_2 followed by air for 6 h. For a comparison, gallium-free MCM-48 as well as Na-AlMCM-41, Na-FeMCM-41, Na-GaMCM-41, Na-AlMCM-48, Na-FeMCM-48, Na-BMCM-41 and Na-BMCM-48 were also prepared according to a procedure described elsewhere [16,28–34].

2.3. Preparation of H-GaMCM-48

The protonated form of GaMCM-48 was prepared from the sodium form of the calcined sample, Na-GaMCM-48, by ion-exchange. NH_4-GaMCM-48 was first obtained by repeated exchange of Na-GaMCM-48 with 1 M NH_4NO_3 solution at 353 K for 6 h. The H-GaMCM-48 was then obtained by deammoniation at 823 K for 6 h in air.

2.4. Characterization

All the samples were characterized by powder X-ray diffraction (XRD; Rigaku), N_2 sorption isotherm (Sorptomatic-1990), simultaneous thermogravimetry-differential thermal analysis (TG-DTA; Shimadzu DT-30), Fourier transform infrared (FT-IR; Nicolet Impact 400) spectroscopy, ^{29}Si and ^{71}Ga magic angle spinning-nuclear magnetic resonance (^{29}Si MAS-NMR: Varian VXR-300S; ^{71}Ga MAS-NMR: Bruker Avance DPX 300) and inductively coupled plasma-atomic emission spectroscopy (ICP-AES; Labtam Plasma 8440). The surface area was estimated using the Brunauer–Emmett–Teller (BET) method and the pore size was calculated by Barrett–Joyner–Halenda (BJH) formula [35]. The pore volume was determined from the amount of N_2 adsorbed at $P/P_0 = 0.5$. TEM and ED analysis was carried out on Philips CM 200 operating at 200 kV (structural resolution of 0.23 nm). The image and ED were recorded with GATAN CCD-camera. Calcined GaMCM-48 samples were used for TEM and ED studies. Samples were dispersed in ethanol with sonication (Oscar ultra sonics), and a drop of it was placed on a carbon coated grid (300 mesh; Sigma–Aldrich).

2.5. Temperature programmed desorption of ammonia

The acidity of the H-GaMCM-48 catalyst was studied by temperature programmed desorption of ammonia (NH_3-TPD). About 200 mg of H-GaMCM-48 was placed in a quartz reactor and was activated at 823 K in air for 6 h, followed by 2 h in helium with a flow rate of 50 ml min^{-1}. The reactor was then cooled to 373 K and maintained for another hour under the same condition. The desorption of ammonia was carried out by heating the reactor up to 823 K at a uniform rate of 10 K min^{-1}. The amount of ammonia desorbed was estimated with the aid of thermal conductivity detector response factor for ammonia.

2.6. Tertiary butylation of phenol

The *t*-butylation reaction of phenol was carried out ambient pressure using 750 mg of H-GaMCM-48 catalyst (100–120 mesh) in a fixed-bed continuous flow glass reactor (i.d. = 6.0 mm). Prior to the reaction, the catalyst was activated at 773 K in flowing air for 8 h followed by cooling to reaction temperature (448 K) under nitrogen flow of ca. 50 ml/min. After an hour, the reactant mixture, i.e. phenol and *t*-butyl alcohol, with a desired (molar) ratio and weight hour space velocity (WHSV) was fed into the reactor using a liquid injection pump (Sigmamotor) with nitrogen as carrier gas. The gaseous products were collected in cold traps, and analyzed at 30 min intervals.

2.7. Products analyses

The various products of the *t*-butylation reaction, viz., *o-t*-BP, *m-t*-BP, *p-t*-BP, and 2,4-di-*t*-BP, were identified by gas chromatography (NUCON 5700) with SE-30 and AT1000 columns. In addition, all these products were confirmed with the use of a combined gas chromatography-mass spectrometry (GC-MS; HEWLETT G1800A) set-up fitted with HP-5 capillary column.

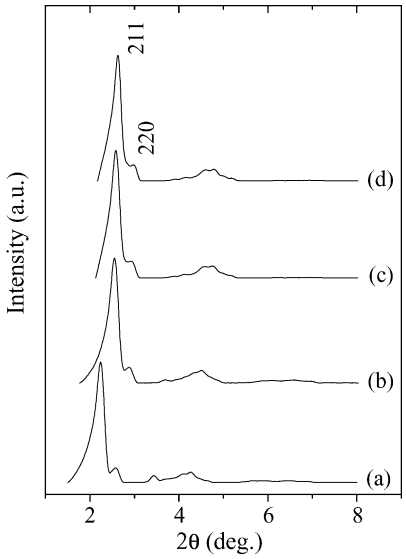

Fig. 1. XRD patterns of GaMCM-48(30): (a) as-synthesized; (b) calcined; (c) protonated; (d) after reaction.

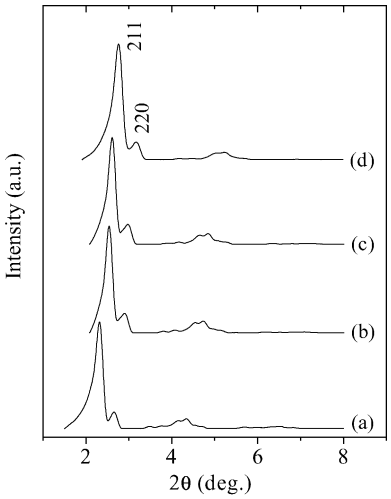

Fig. 3. XRD patterns of GaMCM-48(90): (a) as-synthesized; (b) calcined; (c) protonated; (d) after reaction.

3. Result and discussion

Figs. 1–3 show the XRD patterns of several GaMCM-48 with different Si/Ga (molar) ratios. The diffraction patterns show all the major reflections, which are characteristic of a cubic MCM-48 structure [1,6]. The calculated average unit cell parameter (a_0), Si/Ga ratio and N_2 sorption analyses for various GaMCM-48 samples are given in Table 1. XRD data clearly indicate an increase in unit cell dimension as the gallium content increases in the samples, which could be accounted for the isomorphous substitution of trivalent gallium to tetravalent silicon owing to the larger crystal radius of former (0.62 Å) than latter (0.40 Å) [36]. Indeed, a similar unit cell expansion can also be noticed for AlMCM-48 as well as FeMCM-48, while for BMCM-48 a decrease in the dimension can be observed (see Table 1). Such an observation is in line with the crystal radii of the substituent ions in the silicate framework structure (see also Table 2). Fig. 4 shows the XRD patterns of MeMCM-41 (Me = Ga, Al, Fe and B) samples, and that the diffraction patterns are typical of a hexagonal MCM-41 structure [1,6]. Table 2 summarizes the a_0 values, Si/Me ratios and N_2 sorption data for various MeMCM-41 along with MCM-41.

ICP-AES data of Na-GaMCM-48 indicate that the gallium content in the catalyst remains nearly the same or close to the starting (gel) composition. This suggests the complete incorporation of gallium in the silicate matrix (Table 1). N_2 adsorption–desorption isotherms for all GaMCM-48 sample show type IV isotherms, which are characteristic for mesoporous materials [37]. A sharp inflection in the relative pressure (P/P_0) range 0.2–0.4 corresponds to capillary condensation within uniform mesopores. The pore volume,

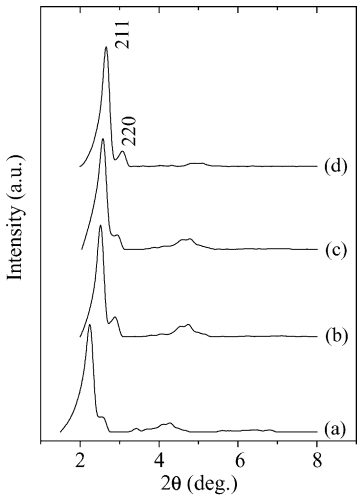

Fig. 2. XRD patterns of GaMCM-48(60): (a) as-synthesized; (b) calcined; (c) protonated; (d) after reaction.

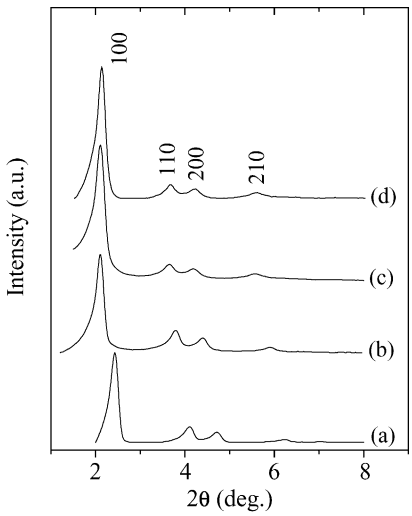

Fig. 4. XRD patterns of: (a) BMCM-41(60); (b) AlMCM-41(60); (c) GaMCM-41(60); (d) FeMCM-41(50).

Table 1
XRD, ICP-AES, and N_2 sorption analysis results of various Na-MeMCM-48 (Me = Al, Ga, Fe and B) samples

Catalyst[a]	(a_0/Å)[b]		Si/Me (molar) ratio[c]		N_2 sorption data		
	Synthesized catalyst	Calcined catalyst	Synthesis gel	Calcined catalyst	Pore volume (ml g^{-1})	Pore diameter (Å)	Surface area (m^2 g^{-1})
MCM-48	92.72	80.07	–	–	0.85	34	1220
GaMCM-48(90)	94.12	83.96	90	92	0.80	32	1080
GaMCM-48(60)	96.89	86.12	60	61	0.79	30	1050
GaMCM-48(30)	97.92	87.03	30	29	0.75	28	980
AlMCM-48(60)	96.89	88.07	60	62	0.80	30	1060
FeMCM-48(50)	96.95	86.77	50	75	0.74	28	860
BMCM-48(60)	92.60	80.02	60	62	0.72	27	890

[a] Number in parenthesis is Si/Me molar ratio in synthesis gel.
[b] Average unit cell parameter (a_0) calculated using $1/d = \sqrt{h^2} + k^2 + l^2/a$.
[c] ICP-AES.

Table 2
XRD, ICP-AES, and N_2 sorption analysis results of various Na-MeMCM-41 (Me = Al, Ga, Fe and B) samples

Catalyst[a]	Crystal radii (Å)[b]	a_0 (Å)[c]		Si/Me (molar) ratio[d]		N_2 sorption data		
		Synthesized catalyst	Calcined catalyst	Synthesis gel	Calcined catalyst	Pore volume (ml g^{-1})	Pore diameter (Å)	Surface area (m^2 g^{-1})
MCM-41	0.40[e]	46.64	43.56	–	–	0.80	30	1060
BMCM-41(60)	0.25	46.02	42.89	60	63	0.70	25	820
AlMCM-41(60)	0.53	49.28	47.88	60	58	0.76	28	1020
GaMCM-41(60)	0.61	50.75	48.47	60	54	0.73	27	980
FeMCM-41(50)	0.63	55.05	49.09	50	75	0.74	28	860

[a] Number in parenthesis is Si/Me molar ratio in synthesis gel.
[b] Trivalent metal ion in tetrahedral environment [36].
[c] Average unit cell parameter (a_0) calculated using $1/d^2 = 4/3(h^2 + hk + k^2/a^2)$.
[d] ICP-AES data.
[e] Tetravalent silicon in tetrahedral environment [36].

surface area, and pore diameter deduced from the N_2 adsorption isotherm for GaMCM-48 samples are presented in Table 2. These results clearly support the mesoporous nature of the GaMCM-48 catalyst. The TEM image of calcined GaMCM-48 indicates that the mesopores are arranged along the (1 1 0) plane [38], and the ED pattern confirms the good quality of the sample [39].

TG-DTA of the as-synthesized Na-GaMCM-48 (Fig. 5) shows a total weight loss of about 55–60% (in three steps), which is typical of mesoporous MCM-48 [9]. The observed (three) different weight losses correspond to the removal of adsorbed water and/or gas molecules (<373 K; 5–7%), oxidative degradation of template molecules (393–725 K; 45–47%), and condensation (dehydroxylation) of silanol groups (>773 K; 5–6%). It can be seen from Fig. 5 that the TG results are well supported by the respective endothermic and/or exothermic transitions in DTA. On the other hand, TG of calcined Na-GaMCM-48 (not reproduced here) gave a 25% weight loss while the protonated samples (before and after reaction) showed a weight loss of 20–22%. The corresponding endothermic transitions in the range 353–363 K confirm the desorption of adsorbed species. This indicates a hydrophilic nature of GaMCM-48.

Fig. 6 depicts the ^{71}Ga MAS-NMR spectra of as-synthesized Na-GaMCM-48, which shows a strong signal at 148–160 ppm corresponding to tetrahedral gallium in the framework MCM-48 structure [9,20–22]. Indeed, similar ^{71}Ga MAS-NMR spectra have been reported for various Ga-substituted microporous [40,41] and mesoporous [20–23,43] molecular sieves. On the other hand, ^{29}Si MAS-NMR spectra of as-synthesized and calcined

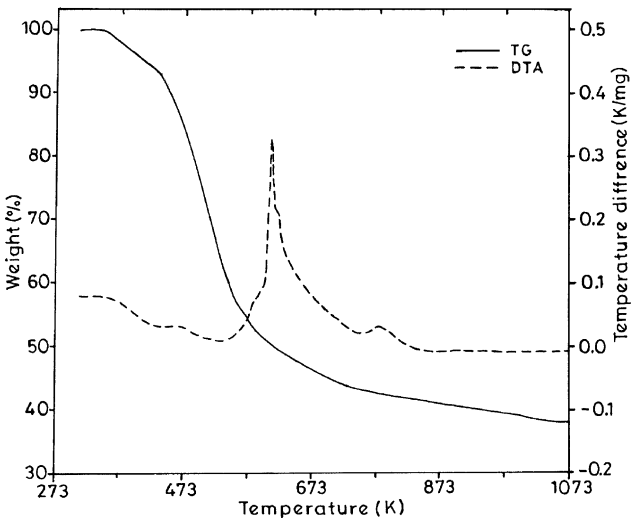

Fig. 5. TG-DTA spectra of as-synthesized Na-GaMCM-48.

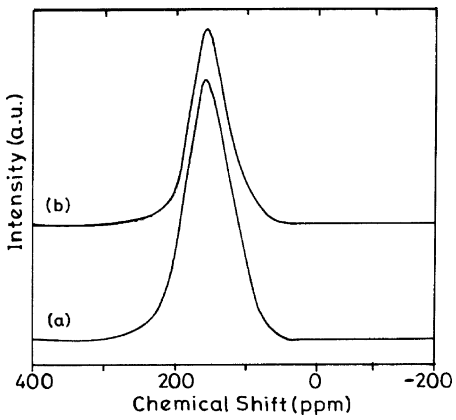

Fig. 6. ^{71}Ga MAS-NMR spectra of: (a) Na-GaMCM-48(30) and (b) Na-GaMCM-48(60).

Na-GaMCM-48 [34] gave two main signals (not reproduced here) centered at −108.5 ppm, assigned to Q_4 site [$Si(OSi)_4$], and −99.5 ppm, assigned to Q_3 site [$Si(SiO)_3(OH)$], with a weak shoulder at −90.1 ppm attributed to Q_2 site [$Si(OSi)_2(OH)_2$] [42]. However, upon calcination, the intensity of Q_4 signal increases indicating further condensation of silanol groups resulting in the formation of siloxane (Si–O–Si) bonds.

Fig. 7 depicts the NH_3-TPD profiles of various H-GaMCM-48. The ammonia desorption trace was deconvoluted using Gaussian functions with the temperature as variant. The deconvoluted traces of the NH_3-TPD profiles were assigned on the basis of literature reports [16,21,28,32]. The first peak, around 420–440 K, referred to as type (i) is attributed to surface hydroxyl groups (weak acid sites), whereas the next two peaks, types (ii) and (iii) in the range 450–480 and 540–600 K, originate from moderate and strong structural (Brønsted) acid sites, respectively, due to the presence of tetrahedral gallium in two different framework sites. The broad and weak peak around 650–700 K, designated as type (iv), is attributed to weak Lewis acid sites, which may arise from tri-coordinated gallium in the framework. A further increase in temperature (750 K) resulted in a weak peak, which may be assigned to non-structural Lewis acid sites originating from the non-framework gallium species. However, for the Si/Ga = 30, a significant decrease in the type (iii) acid site is noticed. This observation could be attributed to the presence of types (iv) and (v) sites as a consequence of the formation of octahedral gallium ions. It is also clear from Fig. 7 that the area under the profiles corresponding to the moderate and strong Brønsted acid sites has a much larger contribution (50–70%), which is favorable for the chosen reaction.

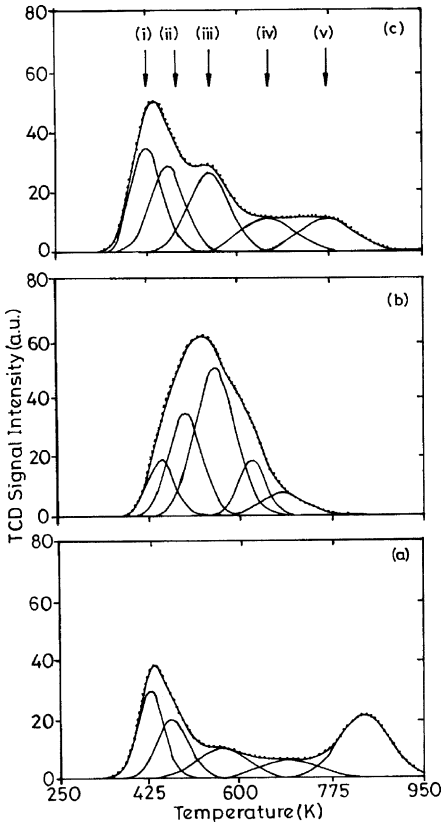

Fig. 7. Ammonia TPD profile of: (a) H-GaMCM-48(30); (b) H-GaMCM-48(60); (c) H-GaMCM-48(90).

Table 3 presents the results of *t*-butylation of phenol over H-GaMCM-48 under optimized experimental conditions. For comparison, we have also included the results of H-BMCM-41, H-AlMCM-41, H-GaMCM-41, H-FeMCM-41, H-BMCM-48, H-AlMCM-41 and H-FeMCM-48. It is interesting note from this table that, in general, the phenol conversion is higher for the MCM-48 structure than the corresponding MCM-41 structure. The observed higher conversion of the former may be attributed to the three-dimensional pore system of MCM-48 structure compared to the one-dimensional pore system of MCM-41 structure [7,12,19], as well as to the larger amount of moderate-to-strong Brønsted acid sites in the former. However, the increased activity may simply reflect the increase in surface area of the MCM-48 structure. We did not observe any trend in the selectivity of *p*-*t*-butyl phenol for both these structure types. Interestingly, the H-GaMCM-48 catalyst is more stable. And deactivates only after about 10 h, while all others show a loss of activity already after about 3 h. Pu et al. [19] have reported a similar observation for isopropylation of naphthalene and pyrene over AlMCM-41 and AlMCM-48. Thus, the present study clearly demonstrates the advantage of three-dimensional pore system of MCM-48 structure over one-dimensional pore structure of MCM-41 structure for the chosen reaction.

Table 4 summarizes the results of the phenol reaction over H-GaMCM-48 with different Si/Ga ratios under optimized experimental conditions. As can be seen from the table, the phenol conversion increases with increase in gallium content, i.e. from (Si/Ga ratio) 90 to 60. The observed increase in conversion could be attributed to an increase in moderate and strong acid sites (Fig. 7), i.e. types (ii) and (iii). In addition, the increase in activity may also be explained

Table 3
Tertiary butylation of phenol over various mesoporous metallosilicates[a]

Reactant/products	H-GaMCM-48	H-GaMCM-41	H-AlMCM-48	H-AlMCM-41	H-FeMCM-41	H-FeMCM-48	H-BMCM-48	H-BMCM-41
Conversion (wt.%)	63.6	55.2	59.1	35.9	21.1	27.6	13.5	8.9
Selectivity (wt.%)								
o-*t*-BP	10.1	12.3	8.1	8.1	9.5	9.8	30.2	36.9
m-*t*-BP	2.9	3.6	2.5	4.7	–	–	–	–
p-*t*-BP	76.5	71.4	79.8	83.3	87.0	87.8	69.8	63.1
2,4-di-*t*-BP	10.5	12.7	9.6	3.9	3.5	2.4	–	–

[a] Reaction conditions: $T = 448\,K$; WHSV $= 4.8\,h^{-1}$; TOS $= 1.5\,h$; *t*-BA:phenol = 2:1.

Table 4
Effect of Si/Ga (molar) ratio on the tertiary butylation of phenol reaction[a]

Reactant/products	H-GaMCM-48(30)	H-GaMCM-48(60)	H-GaMCM-48(90)
Conversion (wt.%)	45.9	63.6	42.2
Selectivity (wt.%)			
o-*t*-BP	10.4	10.1	8.9
m-*t*-BP	1.9	2.9	2.3
p-*t*-BP	72.7	76.5	80.9
2,4-di-*t*-BP	15.9	10.5	8.4

[a] Reaction conditions: $T = 448\,K$; WHSV $= 4.8\,h^{-1}$; TOS $= 1.5\,h$; *t*-BA:phenol = 2:1.

based on the differences in the surface area of the catalysts (see Table 1). The results are in excellent agreement with our earlier results on mesoporous H-GaMCM-41 [32] and H-AlMCM-41 [44]. However, with a further increase in gallium content, i.e. Si/Ga = 30, both the (phenol) conversion and the (*p*-*t*-BP) selectivity decrease, possibly due to dealkylation of *p*-*t*-BP and/or a secondary alkylation reaction. This is well supported by the observed increase in 2,4-di-*t*-BP. Only marginal or no activity was observed for the gallium-free MCM-48 and MCM-41 structures. Finally, it is also interesting to note that the diffraction patterns of the spent catalyst (see Figs. 1d, 2d and 3d) remains nearly the same as that of the initial catalyst, i.e. before the reaction indicating the structural stability of catalysts even after the reaction.

4. Conclusion

In summary, in the present investigation, we have successfully demonstrated the synthesis and characterization of high quality GaMCM-48. Further, we have also showed that the protonated catalyst, i.e. H-GaMCM-48, exhibits higher activity for the *t*-butylation of phenol than many other catalysts reported so far, and that this catalyst displays much higher activity than the analogous H-BMCM-48, H-AlMCM-48 and H-FeMCM-48 as well as the corresponding one-dimensional H-MeMCM-41 (Me = B, Al, Ga and Fe). Moreover, the deactivation was found to be lower owing to three-dimensional pore structure, and hence this catalyst displays superior performance. In addition, it was also deduced from this study that the increased in activity of H-GaMCM-48 could be due to the presence of large amount of moderate-to-strong Brønsted acid sites as compared to many other molecular sieves-based systems.

Acknowledgements

The authors thank RSIC/SAIF, IIT-Bombay for TEM, ^{29}Si MAS-NMR and ICP-AES facilities, and Instrumentation Center, IISc, Bangalore for ^{71}Ga MAS-NMR. The authors also thank Dr. A. Sakthivel for the initial work as well as for the experimental assistance.

References

[1] C.T. Kresge, M.E. Leonowicz, W.J. Roth, J.C. Vartuli, J.S. Beck, Nature 359 (1992) 710;
J.S. Beck, J.C. Vartuli, W.J. Roth, M.E. Leonowicz, K.D. Schmidt, C.T.-W. Chu, D.H. Olson, E.W. Sheppard, S.B. McCullen, J.B. Higgins, J.L. Schlenker, J. Am. Chem. Soc. 114 (1992) 10834.
[2] A. Sayari, Chem. Mater. 8 (1996) 1840.
[3] A. Corma, Chem. Rev. 97 (1997) 2373.
[4] J.Y. Ying, C.P. Mehnert, M.S. Wong, Angew. Chem. Ind. Edit. 38 (1999) 56.
[5] On.D. Trong, D. Desplantier-Giscard, C. Danumah, S. Kaliaguine, Appl. Catal. A 222 (2001) 299.
[6] P. Selvam, S.K. Bhatia, C. Sonwane, Ind. Eng. Chem. Res. 40 (2001) 3237.
[7] K.A. Koyano, T. Tatsumi, J. Chem. Soc., Chem. Commun. (1996) 145.
[8] W. Zhang, T.J. Pinnavaia, Catal. Lett. 38 (1996) 261.
[9] H. Kosslick, G. Lischke, H. Landmesser, B. Parlitz, W. Storek, R. Fricke, J. Catal. 176 (1998) 102.
[10] H. Landmesser, H. Kosslick, U. Kurschner, R. Fricke, J. Chem. Soc., Faraday Trans. 94 (1998) 971.
[11] X. Auvray, C. Petipas, R. Anthore, I. Rico, A. Lattes, J. Phys. Chem. 93 (1989) 7458.
[12] W. Zhao, Y. Luo, P. Deng, Q. Li, Catal. Lett. 73 (2001) 199.
[13] A. Sakthivel, S.E. Dapurkar, P. Selvam, Catal. Lett. 77 (2001) 155.
[14] A. Sakthivel, S.E. Dapurkar, P. Selvam, Appl. Catal. A 246 (2003) 283.
[15] S.E. Dapurkar, A. Sakthivel, P. Selvam, New J. Chem. 27 (2003) 1184.
[16] S.E. Dapurkar, P. Selvam, Appl. Catal. A 254 (2003) 239.
[17] K. Vidya, S.E. Dapurkar, P. Selvam, S.K. Badamali, D. Kumar, N.M. Gupta, J. Mol. Catal. A 181 (2002) 91;
K. Vidya, S.E. Dapurkar, P. Selvam, S.K. Badamali, D. Kumar, N.M. Gupta, J. Mol. Catal. A 191 (2003) 149.

[18] E. Armengol, A. Corma, H. Garcia, J. Primo, Appl. Catal. A 149 (1997) 411.
[19] S.B. Pu, J.B. Kim, M. Seno, M.T. Inui, Microporous Mater. 10 (1997) 25.
[20] C.-F. Cheng, H. He, W. Zhou, J. Klinowski, J.A.S. Goncalves, L.F. Gladden, J. Phys. Chem. 100 (1996) 390.
[21] H. Kosslick, G. Lischke, G. Walther, W. Storek, A. Martin, R. Fricke, Microporous Mater. 9 (1997) 13;
H. Kosslick, H. Landmesser, R. Fricke, J. Chem. Soc., Faraday Trans. 93 (1997) 1849;
H. Kosslick, G. Lischke, B. Parlitz, W. Storek, R. Fricke, Appl. Catal. A 184 (1999) 49.
[22] K. Okumura, K. Nishigaki, M. Niwa, Chem. Lett. (1998) 749;
K. Okumura, K. Nishigaki, M. Niwa, Micropor. Mesopor. Mater. 4445 (2001) 509.
[23] R. Fricke, H. Kosslick, G. Lischke, M. Richter, Chem. Rev. 100 (2000) 2303.
[24] A. Sakthivel, P. Selvam, Bull. Catal. Soc. India 1 (2002) 41.
[25] E.H. Knözinger, J. Weitkamp, Handbook of Heterogeneous Catalysis, vol. 5, VCH, Weinheim, 1997;
J.H. Clark, D.J. Macquarrie, Org. Process Res. Dev. 1 (1997) 149.
[26] K. Zhang, H. Zhang, G. Xu, S. Xiang, D. Xu, S. Liu, H. Li, Appl. Catal. A 207 (2001) 183.
[27] C.D. Chang, S.D. Hellring, US Patent 5 288 927 (1994).
[28] S. Subramanian, A. Mitra, C.V.V. Satyanarayana, D.K. Chakrabarty, Appl. Catal. A 229 (1997) 159.
[29] A. Sakthivel, S.K. Badamali, P. Selvam, Micropor. Mesopor. Mater. 39 (2000) 457.
[30] S.K. Badamali, A. Sakthivel, P. Selvam, Catal. Today 63 (2000) 291.
[31] S.K. Badamali, A. Sakthivel, P. Selvam, Catal. Lett. 65 (2000) 153.
[32] A. Sakthivel, P. Selvam, Catal. Lett. 84 (2002) 37.
[33] S.E. Dapurkar, S.K. Badamali, P. Selvam, Catal. Today 68 (2001) 63.
[34] S.E. Dapurkar, Ph.D. Thesis, IIT-Bombay, 2004.
[35] E.P. Barrett, L.G. Joyner, P.P. Halenda, J. Am. Chem. Soc. 73 (1951) 373.
[36] R.D. Shannon, C.T. Prewitt, Acta. Crystallogr. B 25 (1969) 925.
[37] K.S.W. Sing, D.H. Everett, R.A.W. Haul, L. Mosenu, R.A. Pierotti, J. Rouquerol, T. Siemieniewska, Pure Appl. Chem. 57 (1985) 603.
[38] R. Schmidt, M. Stöcker, M.D. Akporiaye, E.H. Tørstad, A. Olsen, Microporous Mater. 5 (1995) 1.
[39] A. Carlsson, M. Kaneda, Y. Sakamoto, O. Terasaki, R. Ryoo, S.H. Joo, J. Electron Microsc. 48 (1999) 795.
[40] C.H.C. Timken, E. Oldfied, J. Phys. Chem. 109 (1987) 7669.
[41] E. Lalik, X. Liu, J. Klinowski, J. Phys. Chem. 96 (1992) 805.
[42] C.Y. Chen, H.-X. Li, M.E. Davis, Microporous Mater. 2 (1993) 17.
[43] A. Tuel, S. Gontier, Chem. Mater. 8 (1996) 114.
[44] A. Sakthivel, S.E. Dapurkar, N.M. Gupta, S.K. Kulshreshtha, P. Selvam, Micropor. Mesopor. Mater. 65 (2003) 177.